HHS Public Access

Author manuscript

Neuroimage. Author manuscript; available in PMC 2019 January 01.

Published in final edited form as:

Neuroimage. 2018 January 01; 164: 131–143. doi:10.1016/j.neuroimage.2016.11.039.

Techniques for blood volume fMRI with VASO: From low-resolution mapping towards sub-millimeter layer-dependent applications

Laurentius Huber[a,*], **Dimo Ivanov**[b], **Daniel A. Handwerker**[a], **Sean Marrett**[c], **Maria Guidi**[d], **Kāmil Uludağ**[b], **Peter A. Bandettini**[a,c], and **Benedikt A. Poser**[b]

[a]Section on Functional Imaging Methods, Laboratory of Brain and Cognition, NIMH, NIH, Bethesda, MD, USA [b]Maastricht Brain Imaging Centre, Faculty of Psychology and Neurosciencve, Maastricht University, Maastricht, The Netherlands [c]FMRIF, NIMH, NIH, Bethesda, MD, USA [d]Max Planck Institute for Human Cognitive and Brain Sciences, Leipzig, Germany

Abstract

Quantitative cerebral blood volume (CBV) fMRI has the potential to overcome several specific limitations of BOLD fMRI. It provides direct physiological interpretability and promises superior localization specificity in applications of sub-millimeter resolution fMRI applications at ultra-high magnetic fields (7 T and higher). Non-invasive CBV fMRI using VASO (vascular space occupancy), however, is inherently limited with respect to its data acquisition efficiency, restricting its imaging coverage and achievable spatial and temporal resolution. This limitation may be reduced with recent advanced acceleration and reconstruction strategies that allow two-dimensional acceleration, such as in simultaneous multi-slice (SMS) 2D-EPI or 3D-segmented-EPI in combination with CAIPIRINHA field-of-view shifting. In this study, we sought to determine the functional sensitivity and specificity of these readout strategies with VASO over a broad range of spatial resolutions; spanning from low spatial resolution (3 mm) whole-cortex to sub-millimeter (0.75 mm) slab of cortex (for cortical layer-dependent applications). In the thermal-noise-dominated regime of sub-millimeter resolutions, 3D-segmented-EPI-VASO provides higher temporal stability and sensitivity to detect changes in CBV compared to 2D-EPI-VASO. In this regime, 3D-segmented-EPI-VASO unveils task activation located in the cortical laminae with little contamination from surface veins, in contrast to the cortical surface weighting of GE-BOLD fMRI. In the physiological-noise-dominated regime of lower resolutions, however, 2D-SMS-VASO shows superior performance compared to 3D-segmented-EPI-VASO. Due to its superior sensitivity at a layer-dependent level, 3D-segmented-EPI VASO promises to play an important role in future neuroscientific applications of layer-dependent fMRI.

[*]Corresponding author: Laurentius Huber, PhD Section on Functional Imaging Methods, NIMH, National Institutes of Health Building 10, Room 1D80B 10 Center Dr. MSC 1148 Bethesda, MD 20892-1148. Tel.: +1 301 402 7298. Laurentius.Huber@nih.gov.

Keywords

vascular space occupancy; SS-SI VASO; cerebral blood volume; simultaneous multi-slice; 3D-EPI; 7 Tesla MRI; layer-dependent fMRI

1. Introduction

A detailed understanding of the organization of macroscopic brain areas into distinct networks requires a profound knowledge about the inter-area connections into functional building blocks of small cortical layers (Yacoub et al., 2015). The cortical grey matter (GM) ribbon consists of up to 6 of these histologically-defined cortical layers with thicknesses usually between 0.2 mm and 1 mm. Mapping the brain activity across thin cortical layers and their differential functional connectivity to distant brain areas would be highly valuable for human cognitive research. The only non-invasive *in vivo* imaging method currently capable of mapping brain activity at sub-millimeter resolutions, and hence having the potential ability to detect layer-dependent physiological signal changes, is functional magnetic resonance imaging (fMRI).

Conventional blood oxygenation level dependent (BOLD) fMRI methods, however, are most commonly applied at relatively coarse resolutions in the range of 2 – 4 mm. To increase the resolution to the sub-millimeter range (e.g. 0.75 mm), there are two major challenges that need to be addressed: First, the corresponding reduction in voxel volume of up to two orders of magnitude limits the available MRI signal-to-noise ratio (SNR) and, thus, sensitivity to detect signal changes (contrast to noise ratio, CNR). Second, the BOLD-relevant oxygenation changes in draining veins (Menon et al., 1995; Turner, 2002) result in a reduced effective spatial resolution, independent of the nominal imaging resolution used. Engel at al. could qnatify the spatial resolution of fMRI at 1.5 T in retinotopy studies of the human visual cortex to be consistent with an area whose full width at half maximum (FWHM) spreads across 3.5 mm (Engel et al., 1997). At 3 T, Parkes et al. could quantify the FWHM of conventional GE-BOLD and SE-BOLD with a rotating visual wedge paradigm to be 3.9 mm and 3.4 mm, respectively. Shmuel et al. investigated the regional specificity of BOLD fMRI at 7T in a flat (unfolded) region in V1. They found that, when the large veins are removed from the analysis, the FWHM of GE-BOLD is about 2 mm (1.52 mm shortly after stimulus onset and 2.42 mm 5 seconds after stimulus onset).

It has been shown in animals e.g. (S.-G. Kim et al., 2013; Smirnakis et al., 2007) and in humans (Huber et al., 2015a) that fMRI contrasts based on cerebral blood volume (CBV) can map changes of brain activity with higher spatial specificity and without contamination of the remote draining veins compared to BOLD fMRI.

The most commonly used method for non-invasive measurements of CBV changes in humans is vascular space occupancy (VASO) (Lu et al., 2003). VASO takes advantage of the T_1 difference between blood and surrounding tissue, and uses an inversion recovery pulse sequence to null blood signal while maintaining part of the tissue signal. The VASO signal intensity can thus be considered proportional to 1-CBV. When neural activation causes CBV to increase, the VASO signal will show a decrease, allowing the detection of activated

regions in the brain (Lu and van Zijl, 2012). VASO is particularly attractive at high fields (7 T) due to the increase in image SNR and the longer longitudinal relaxation time of blood, which can amplify VASO's functional T_1-contrast (Huber et al., 2014b). However, as the VASO contrast relies on elimination of the intravascular signal, it requires image acquisition after an inversion pulse has been applied at the blood magnetization nulling time. Dependent on the VASO variant used, the blood nulling time does not only depend on blood's T_1, but also on the dynamic steady-state of the sequence including the respective flip angles and TRs. Independent of the VASO variant used, there is only a short acquisition window of blood nulling to acquire the signal. Hence, if multiple consecutive slices are acquired after each inversion, they end up with different inversion times (TI), allowing only a small number of slices to be acquired, which limits the achievable brain coverage of VASO using standard EPI readout. To increase the imaging coverage without unacceptable penalties in image quality, VASO has been combined with other readout strategies at 3 T, for instance, 3D-GRASE, TFL/FFE, and 3D-HASTE (Cheng et al., 2014b; Lu et al., 2004; Poser and Norris, 2011, 2009).

Significant gains in both spatial resolution and spatial coverage at ultra-high field without compromising SNR losses may be achieved by incorporating recent improvements in accelerated acquisition techniques. In terms of sampling efficiency, the most important innovation since the introduction of EPI itself is EPI with simultaneous multi-slice imaging (SMS). SMS uses multi-band (MB) excitations to simultaneously excite multiple slices and use the coil sensitivity profiles to disentangle the signals from the different slices (Feinberg and Setsompop, 2013; Feinberg et al., 2010; Larkman et al., 2001; Moeller et al., 2010). As a result, the volume acquisition time is reduced by the nominal slice acceleration factor. Together with blipped-CAIPIRIHA sampling, SMS-EPI has been shown to achieve high slice and in-plane acceleration factors with minimal g-factor penalty (a measure of SNR loss in accelerated acquisition schemes (Setsompop et al., 2012)). SMS-EPI was rapidly adopted in all MRI modalities based on 2D-EPI readout, including BOLD (Feinberg et al., 2010), diffusion (Setsompop et al., 2012), CBF (Feinberg et al., 2013; Ivanov et al., 2016a; T. Kim et al., 2013) and CBV imaging (Huber et al., 2016a).

An alternative to sequential 2D multi-slice imaging is volumetric 3D-segmented-EPI (Poser et al., 2010) acquisition, which allows equivalent acquisition speedup and can also be combined with CAIPIRINHA sampling (Narsude et al., 2016; Poser et al., 2013) to yield g-factor benefits that are analogous to SMS-EPI (Zahneisen et al., 2015, 2014).

Earlier work at 3 and 7 T has investigated the relative merits of 2D and 3D acquisitions for BOLD fMRI (Lutti et al., 2013; Stirnberg et al., 2016), but neither did so systematically at different spatial resolutions nor below 1 mm^3. For high resolution, low image SNR acquisitions, the inherent SNR advantage of volumetric acquisition may become an important contribution in pushing the spatial boundaries of fMRI applications. This SNR adavantage is coming from the fact that volumetric slab-excitation allows the whole magnetization to be acquired several times in a time scale that is approaching the relaxation times.

In this paper, we discuss and investigate the limitations and the applicability of CBV fMRI from resolutions of 3 mm to 0.75 mm (layer-dependent). Specifically, we focus on the relative amounts of thermal and physiological noise, and signal stability with decreasing voxel sizes, and local specificity to cortical layers.

Aiming towards layer-dependent neuroscience applications, we compare gradient echo (GE) BOLD and CBV-VASO contrast mechanisms and 2D-SMS and 3D-segmented-EPI readout strategies across a wide range of resolutions. We elaborate on the limitations and challenges specific to sub-millimeter layer-dependent fMRI and show how new approaches, such as 3D-segmented-EPI VASO, hold promise to cope with them.

2. Materials and Methods

2.1. MR sequence and setup

Ten healthy right-handed volunteers (age 22–42 years) participated after granting informed consent under an NIH Combined Neuroscience Institutional Review Board-approved protocol (93-M-0170) in accordance with the Belmont Report and US Federal Regulations that protect human subjects. Slice-selective slab-inversion (SS-SI) VASO (Huber et al., 2014b) with 2D-SMS and 3D-segmented-EPI readout was implemented on a MAGNETOM 7 T scanner (Siemens Healthcare, Erlangen, Germany) using the vendor provided IDEA environment (VB17A-UHF). For RF transmission and reception, a single-channel-transmit/32-channel receive head coil (Nova Medical, Wilmington, MA, USA) was used. The scanner was equipped with a SC72 body gradient coil (maximum effective gradient strength used here: 49 mT/m; maximum slew rate used: 199 T/m/s). The timing of magnetization preparation and interleaved acquisition of VASO and BOLD data is schematically depicted in Fig. 1(A)–(C). The timing of the acquistions is: $TI_1/TI_2/TR$ = 1100/2600/3000 ms across all experiments. The blood-nulling time is calculated based on the assumed value of blood T_1 = 2100 ms (Grgac et al., 2012; Hales et al., 2015), following earlier VASO studies at 7 T (Huber et al., 2016a, 2014a). The adiabatic VASO inversion pulse is based on the TR-FOCI pulse (Hurley et al., 2010) (Fig. 1(A)–(B)). The pulse duration was 10 ms and the bandwidth was 6.3 kHz. For sequence parameters regarding the signal acquisition (excitation, acceleration, resolution), see the sections below.

VASO can be contaminated by inflow of non-inverted blood, especially when blood T_1 is not much shorter than the TR (Donahue et al., 2009). These inflow effects can be minimized, when the blood-nulling time is shorter than the time that blood needs to arrive from the arteries in the neck to the micro vessels of the imaging slice (Huber et al., 2016a). Here, a TI_1 = 1100 ms was chosen, which includes an additional leeway of 200 ms compared to the estimated arterial arrival time in the sensorimotor cortex (Mildner et al., 2014). The blood-nulling time was manipulated by means of an adjusted inversion efficiency of 87% in a B_1-independent manner by using a phase skip (Fig. 1(A)–(B)) of the RF field during inversion as described in (Huber et al., 2014b). The inversion pulse amplitude was adjusted to have a minimum of 10 μT down to the Circle of Willis across all participants by using a transmitter voltage of 320 V (max during TR-FOCI pulse).

With increasing field strength, the positive BOLD signal change during neural activation increasingly counteracts the negative VASO signal change (Lu and van Zijl, 2005). The GE-BOLD effect typically has two components: intravascular and extravascular. At 7 T, the extravascular BOLD signal dominates the intravascular BOLD signal by more than 90% (Donahue et al., 2010; Uludag et al., 2009). This extravascular BOLD contamination is considerably larger than the desired VASO signal change and needs to be corrected for to obtain quantitative CBV. In SS-SI VASO, an interleaved, pair-wise acquisition (Fig. 1(A)–(B)) of VASO and BOLD images is used to distinguish between BOLD and VASO signal components of the resulting signal. When the pure BOLD contrast contribution is known, the BOLD contamination in the VASO image can be factored out, as described earlier (Huber et al., 2014b).

In order to show the specific challenges of layer-dependent fMRI applications compared to the ones performed at conventional voxel sizes, experiments were conducted at 3 mm, 1.5 mm and 0.75 mm resolutions, for both 3D-segmented-EPI and 2D-SMS-EPI. Seven participants where scanned at each resolution. To obtain best results at the respective resolutions, the FOV, the slice position, and acceleration factors were optimized individually for the 3 mm, 1.5 mm and 0.75 mm protocols, but kept identical for the 2D-SMS VASO and 3D-segmented-EPI acquisitions at each resolution.

These resolution-dependent acquisition parameters are listed as follows:

2.1.1. 3 mm setup: low-resolution whole-cortex coverage case—Whole-cortex coverage was achieved with the following acquisition parameters: 33 tilted axial slices, nominal slice thickness 3 mm, nominal in-plane resolution 3.0 × 3.0 mm^2, TE = 12 ms, partial Fourier = 6/8, in-plane GRAPPA 3, through-plane acceleration 3, CAIPI FOV-shift = 1/2 (was chosen based on the performance in pilot experiments), in-plane phase-encoding direction: anterior-posterior.

2.1.2. 1.5 mm setup: GM-specific application case—24 tilted axial slices were positioned to cover the sensorimotor regions of both hemispheres with: TE = 17 ms, nominal slice thickness 1.5 mm, nominal in-plane resolution 1.5 × 1.5 mm^2, partial Fourier = 6/8, in-plane GRAPPA 2, through-plane acceleration 2, CAIPI FOV-shift = 1/3, in-plane phase-encoding direction: anterior-posterior.

2.1.3. 0.75 mm setup: layer-dependent application case—10 tilted axial slices were positioned to cover the left motor cortex. Slices were rotated until the major region of the thumb representation (next to index finger) was imaged in slices perpendicular to the cortical surface with: TE = 24 ms, nominal slice thickness 1.5 mm, nominal in-plane resolution 0.75 × 0.75 mm^2, in-plane GRAPPA 2, asymmetric matrix size 32 × 96, in-plane phase-encoding direction: left-right. No through-plane acceleration or CAIPI FOV-shifting was applied for this protocol. To minimize T_2^*-blurring, partial Fourier imaging was kept as conservative as possible at 7/8 (Huber et al., 2015c).

2.1.4. Direct comparison across resolutions—Optimal acceleration parameters are highly dependent on the desired resolution, volume coverage and time constraints (TI/TR).

For example, larger FOVs with more slices allow higher acceleration factors than smaller FOVs with only few slices, where the spatial encoding by the coil-array is limited. Moreover, larger voxels allow shorter EPI echo-spacing. Hence, the acquisition/acceleration parameters of the different setups investigated above were optimized differently for the respective resolutions chosen. For a more direct comparison of 2D-SMS and 3D-segmented-EPI readouts, we conducted additional tSNR experiments with identical acceleration parameters and in-plane resolutions, but varying slice thicknesses in 3 participants. Scan parameters were as follows: Matrix: 64 × 64, 8 slices, nominal in-plane resolution 1.0 × 1.0 mm^2, no through-plane GRAPPA, in-plane GRAPPA 2, TE = 24 ms. The slice thickness varied between 0.3 mm and 10 mm.

2.1.5. Investigation of the effect of head motion—In order to investigate the effect of task-correlated head motion in 3D-segmented-EPI and 2D-SMS VASO, we utilized data from 8 experiments in N = 4 participants during a Valsalva breathholding task, which can have a large task-correlated head motion. For imaging, the 1.5 mm protocol was used as described above.

2.2. In-plane acceleration parameters

The acquisition order of the GRAPPA reference lines followed the FLEET approach shown for 2D EPI (Polimeni et al., 2016), and its analogue for 3D-segmented-EPI acquisitions (Ivanov et al., 2015). That is, in-plane segmented reference line acquisition is ordered such that all in-plane (line) segments for a given slice (2D EPI) or k_z-encoding step (3D-segmented-EPI) are acquired in immediate succession before proceeding to the next slice or k_z-encode step. This minimizes segmentation artifacts and results in superior conditioning of the subsequent GRAPPA reconstruction and correspondingly increased tSNR. The vendor's GRAPPA (Griswold et al., 2006) reconstruction algorithms were applied using a 3 × 4 (read direction × phase direction) kernel. Partial Fourier reconstruction (Jesmanowicz et al., 1998) was done with the projection onto convex sets (POCS) algorithm (Haacke et al., 1991) with 8 iterations. Finally, the complex coil images were combined using the vendor's implementation of sum-of-squares.

2.3. 2D-SMS specific parameters

The nominal slice-selective excitation pulse flip angle was 70° with a pulse duration of 2.5 ms. The summation of multi-band sinc-pulses was conducted with optimized phase schedules for minimizing peak RF power (Wong, 2012) (see corresponding pulse shape in Fig. 1(D)). Online reconstruction on the scanner was performed using a combination of the vendor software and the SMS reconstruction as distributed with the MGH blipped-CAIPI C2P (http://www.nmr.mgh.harvard.edu/software/c2p/sms). SMS signals were first un-aliased with an implementation of SplitSlice-GRAPPA with LeakBlock (Cauley et al., 2014) and a 3 × 3 SliceGRAPPA kernel before entering in-plane reconstruction as described above.

2.4. 3D-segmented-EPI specific parameters

The 3D VASO sequence was based on a previous 3D-segmented-EPI implementation (Poser et al., 2010) with support for CAIPIRINHA sampling (Poser et al., 2013). Online reconstruction was performed using a combination of standard scanner software and a

vendor-provided works-in-progress implementation of GRAPPA CAIPIRINHA (Siemens software identifier: IcePAT WIP 571) with kernel size 4 × 3 × 3.

For direct comparability with the 2D-SMS acquisitions, we used the same in-plane readout (for identical distortions and T_2^*-blurring) and no slab-oversampling (for same number of imaging shots per inversion). 3D slice aliasing was minimized using a sharp slab-excitation pulse profile with a bandwidth-time-product of 25.

The need for magnetization inversion and the need for long volume TR in VASO results in 3D-segmented-EPI segments being acquired in a non-steady state. Hence, in order to minimize any T_1-related blurring along the slice direction (Gai et al., 2011), individual excitation pulse flip angles were varied along the train of k_z-planes to ensure similar GM signal for every shot. The last excitation pulse of every readout was chosen to be nominally 90°. To keep a near constant GM signal across *k*-space segments, the flip angles of the preceding segments were adjusted to be respectively smaller. Depending on the number of segments, the first excitation pulse flip angle was desired to be between 16°-22°. For instance, the 0.75 mm protocol, the nominal flip angles adjusted in the sequence code to be: 21.8°, 22.5°, 23.4°, 24.3°, 25.5°, 26.8°, 28.4°, 30.5°, 33.3°, 37.3°, 43.7°, 57.4°, 90.0°). The T_1-relaxation between consecutive excitation pulses was estimated assuming a tissue T_1-value of 1800 ms at 7 T (Wright et al., 2008).

To be most comparable with the 2D-SMS acquisition scheme and obtain identical distortions and T_2^*-blurring, the number of slices in 2D-SMS and the number of segments in 3D-segmented-EPI were kept the same. Thus, in every 3D-segmented-EPI shot, one whole slice of *k*-space was acquired.

2.5. SAR values

The overall energy deposition of the sequence never exceeded 2.1 W/kg, according to the SAR estimation of the vendor. Due to the considerable SAR contribution from the inversion pulse and the high bandwidth-time-product of 25 in 3D-segmented-EPI, the estimated SAR values for 3D-segmented-EPI were not much lower than for the 2D-SMS EPI. The values were 1.9/2.1 W/kg (3D-segmented-EPI/2D-SMS EPI) for the high resolution (0.75 mm) and 1.3/2.1 W/kg for the low resolution (3 mm) protocol.

2.6. fMRI task

The sensitivity of each protocol to functional activation was investigated with a unilateral finger tapping tasks: one-minute blocks (30 s rest and 30 s, paced tapping with 0.75 Hz) repeated 12 times. This resulted in 12-minute acquisitions for each protocol, plus 20 s – 40 s before and after the 12 blocks, respectively.

The effect of task-correlated head motion was investigated with a Vasalva breathholding task. This task consists of breathholding with additional chest pressure increase (Wu et al., 2015). This task has the potential for efficient high CNR mapping of vascular reactivity. However, its application with VASO is often limited with unwanted motion artefacts arising from correlated head tilting, which made it an ideal control for examining head motion.

Each run consisted of 10 breathholding periods of 15 s interspaced with 45 s of paced breathing.

2.7. Data analysis

All MR images were motion corrected using SPM8 (Functional Imaging Laboratory, University College London, UK). The outermost slices were excluded from the analysis to minimize motion artifacts and residual 3D-segmented-EPI related slab fold-over artifacts. Activation GLM analysis was done using FSL FEAT (Version 5.98) (Worsley, 2001) with a cluster threshold of 10 voxels (applied with AFNI (Cox, 1996)). No signal smoothing was applied at any point during the analysis to minimize losses of spatial specificity (Stelzer et al., 2014).

The tSNR was separately estimated for BOLD and VASO time series after respective signal detrending with AFNI (Cox, 1996). The tSNR was computed over 480 time steps (240 for VASO and 240 for BOLD).

The VASO SNR was estimated by the method described for time series imaging (Feinberg et al., 2013; Glover and Lai, 1998): The even- and odd-numbered time points of VASO were separately averaged, and the sum and difference of these two images were calculated. Note, that the even- and odd-numbered time points refer to the same VASO contrast. They do not refer to the interleaved acquisition of VASO and BOLD in the MR sequence. The VASO SNR was calculated as the mean value across M1 ROIs in the sum image divided by the standard deviation across the same region in the difference image. BOLD SNR was calculated analogously by taking the even- and odd-numbered time points of the BOLD time series.

2.8. Layer-analysis

The analysis to plot functional signal changes across cortical depth followed the description in (Huber et al., 2015b). In short: GM-CSF borders and GM-WM borders for the primary motor cortex “hand knob” were manually drawn on the EPI images. Cortical depths were calculated based on the equi-volume principle (Waehnert et al., 2014). No significance thresholding was applied to avoid biases of variable detection thresholds across cortical depth (Goense et al., 2012a).

3. Results

3.1. tSNR across resolutions with optimized parameters

Results of the tSNR across resolutions are shown in Fig. 2 for one representative participant. 2D-SMS VASO has higher tSNR values compared to 3D-segmented-EPI at conventional resolutions of 1.5 mm and 3 mm. In the thermal-noise-dominated regime of sub-millimeter resolutions (0.75 mm), this relationship becomes inverted and 3D-segmented-EPI outperforms the 2D-SMS VASO in terms of tSNR. The mean tSNR values shown in Fig. 2 refer to values averaged over M1 ROIs across participants (N = 7 in Fig. 2(A)–(B)). With the individually optimized acquisition parameters (acceleration factor and FOV) across protocols, tSNR of GM is above 20 throughout all resolutions shown in Fig. 2(A)–(B). This

means that the strong response of a finger tapping task should exceed the detection threshold with a 12 min fMRI experiment (Murphy et al., 2007).

To reveal the tSNR sensitivity across resolutions independent of GRAPPA and bandwidth effects, the signal stability for the same imaging readout ($1mm^2$ in-plane resolution) is depicted for different slice thicknesses in Fig. 2(C). tSNR values refer to the average across all 3 participants acquired with this protocol. The curves for 2D-SMS and 3D-segmented-EPI VASO show an asymptotic behavior that is qualitatively very similar to the ones shown in previous studies that have investigated the tSNR-SNR relationship across resolutions (Murphy et al., 2007; Triantafyllou et al., 2011). To stress that the tSNR saturation is arising from physiological noise contributions, image SNR is depicted in Fig. 2(D). Image SNR does not show the strong saturation at larger voxel volumes and 3D-segmented-EPI has higher values compared to 2D-SMS for each resolution. Figs. 2(E)–(H) depict the same quantities as in Figs. 2(A)–(D) but for the BOLD signal. Please note the different scaling of colorbars and y-axes.

The consistency of theses results across participants can be seen in Fig. 3.

3.2. Sensitivity to detect functional activation

Functional activation maps for the unilateral finger-tapping task are shown in Fig. 4 for one representative subject. The depicted MRI slices are the same as shown in Fig. 2(A)–(B). Simultaneously acquired functional maps of BOLD signal change are included in order to stress the different spatial patterns of BOLD fMRI compared to CBV-fMRI. Note that the quantitative VASO contrast is inverted to obtain estimates of blood volume in units of ml per 100 ml of tissue (Huber et al., 2015a).

For the low resolution of 3 mm, 2D-SMS and 3D-segmented-EPI activation maps show M1 activation in a very similar fashion (Fig. 4(E), (K)). Note that this is the case despite the ≈ 50% higher tSNR in 2D-SMS compared to 3D-segmented-EPI. This is most likely due to the fact that both readout strategies are well above the detection threshold for a finger-tapping task.

At 1.5 mm resolutions, the voxel size approaches the distance between the neighboring GM ribbons of the central sulcus. Hence, the intracortical CBV signal changes of M1 and S1 start to separate into two distinct clusters of voxels (blue arrows in Fig. 4(C), (I)). Due to the presence of large draining veins above the cortical surface, functional activation in GE-BOLD fMRI, on the other hand, appears as one big cluster (blue arrows in Fig. 4(J)).

For layer-dependent fMRI applications of 0.75 mm resolutions, both 2D-SMS VASO (Fig. 4(A)) and 3D-segmented-EPI VASO (Fig. 4(G)) have enough sensitivity to detect tapping-induced activity in M1. Due to the higher SNR in 3D-segmented-EPI VASO layer-dependent activity features are slightly more obvious (green arrow in Fig. 4(G)) compared to the 2D-SMS VASO (Fig. 4(A)). Even though, there might be some layer-dependent features visible in GE-BOLD data (Fig. 4(B), (H)), most of the signal change appears to be dominated from nonspecific superficial veins.

Please, note the different scaling of the functional responses across resolutions and correspondingly different colorbars in Fig. 4. This was done to account for the larger signal changes at high resolutions when partial volume effects are minimized.

3.3. Susceptibility to task-correlated head motion

During Valsalva breathholding tasks, participants showed considerable head motion. Particularly pitch rotation turned out to be highly correlated with the breathholding task. A motion trace of SPM motion estimation is shown in Fig. 5(A) for one representative subject. Such motion can result in considerable motion artefacts during fMRI response evaluation. Fig. 5(B)–(C) show sagittal views of averaged VASO signal intensities across slices. It can be seen in 2D-SMS-VASO that very small deviations of the effective inversion time results in corresponding inhomogeneities in T_1-weighting and signal intensity across slices. This means that any retrospective motion correction will interpolate these signal inhomogeneities across slices. In 3D-segmented-EPI VASO on the other hand, all slices have the same effective inversion time and retrospective motion correction can be applied without the introduction of motion artefacts.

3.4. Bias of baseline vasculature

The sole fact that specific signal variations across cortical depth can be observed, does not prove layer-specificity, when the underlying physiology is unknown. This is established in the field and has been discussed already in the literature (Koopmans et al., 2011, 2010). According to these discussions, the depth-dependent variations in fMRI signal could simply resemble the baseline vascular distribution. Following suggestions in (Goense et al., 2016), we tried to minimize incorrect interpretations due to this bias by applying multi-modal fMRI and directly comparing it to estimates of the baseline vasculature as done in Fig. 6(G)–(H). Since the functional profiles in Fig. 6(C)–(D) are qualitatively different from Fig. 6(G)–(H), the peak fMRI responses can be considered to be caused by task-specific layer-dependent activation, and not by the baseline vasculature distribution.

4. Discussion

The results shown in Figs. 2–3 demonstrate the advantages and disadvantages of VASO and BOLD fMRI with 2D-SMS and 3D-segmented-EPI acquisitions across a broad range of resolutions. The results can be taken as evidence that in the case of layer-dependent applications, the conventional contrast mechanisms and readout strategies that perform very well at 2 – 4 mm spatial resolutions may no longer be the most suitable choice. Instead, less utilized readout strategies, like 3D-segmented-EPI, and fMRI contrasts, like VASO, might provide superior tools for neuroscientific applications that require spatial specificities in the sub-millimeter regime.

4.1. Benefits of 3D-segmented-EPI at high resolutions

3D-EPI acquisition approaches were originally suggested in (Mansfield et al., 1995; Song et al., 1994). In recent years they have gained considerable interest (Gai et al., 2011; Jorge et al., 2013; Langkammer et al., 2015; Lutti et al., 2013; Van Der Zwaag et al., 2012) due to the flexibility of having an additional k-space dimension. For instance, 3D acquisition

strategies allow partial Fourier imaging along the k_z direction to provide reduction in volume TR (Poser et al., 2010). Furthermore, 3D acquisitions allow thin slices without being limited by excitation pulse imperfections (Poser et al., 2010). They are less prone to motion-induced spin-history effects than 2D imaging since the whole slab or volume is always excited, and - importantly - they allow undersampling to be applied along both the in-plane and through-plane phase-encoding directions (Narsude et al., 2016; Poser et al., 2014, 2010). With the incorporations of controlled aliasing, g-factors can be reduced to a minimum (Narsude et al., 2016; Poser et al., 2013), allowing high total acceleration factors and correspondingly fast temporal sampling. Due to the smaller excitation flip angles used in 3D-segmented-EPI compared to 2D-SMS EPI, 3D-segmented-EPI applications have been suggested to be beneficial at high field strengths, where SAR constraints can limit the number of slices and the TR (Gai et al., 2011; Poser et al., 2010).

One likely reason, why 3D-segmented-EPI has not become as widely applied as single shot 2D-SMS EPI, however, comes from the fact that it is more sensitive to physiological noise components: while the very fast acquisition of 2D-SMS-EPI in the range of few tens of ms ‘freezes out’ cardiac- and respiration-induced signal fluctuations, the extended sampling window in 3D-segmented-EPI, of the order of few hundreds of ms, approaches the timescale of physiological variations. These physiological modulations across the *k*-space acquisition can result in increased signal fluctuations all across the entire image space and limit the fMRI sensitivity

In addition to the different physiological noise contributions, that need to be dealt with differently in 3D-EPI (Jorge et al., 2013; Lutti et al., 2013), 2D-EPI and 3D-EPI have different sequence timing requirements due to 3D-EPI relaxation time differences across slices. Inversion recovery 3D-EPI methods that segment volume k-space across TRs (van der Zwaag et al., 2016), can account for this to allow the same flexibility as a 2D readout. However, pulse sequences using these methods are not widely distributed across MRI scanner vendors.

The results of the study presented here confirm this notion and provide evidence that in the physiological-noise-dominated regime of conventional voxel sizes of 1.5–3 mm, 2D-SMS VASO provides higher signal stability compared to 3D-segmented-EPI VASO (Fig. 1(A)–(B)). At ultra-high resolutions, however, in the thermal-noise-dominated regime, the advantage of increased image SNR becomes more important and 3D-segmented-EPI acquisitions become more stable than 2D-SMS approaches (Fig 1(C)).

4.2. 3D-segmented-EPI in inversion recovery sequences

In inversion-recovery sequences such as for VASO or ASL applications, T_1-relaxation processes can affect the image contrast while a volume is being acquired. In 2D-SMS sequences, the individual slice-groups are acquired consecutively. This means that adjacent slices can have different T_1-weightings. For short TIs (< tissue T_1), this can result in different signal intensity across the brain volume imaged (blue arrows in Fig. 1(A)), with resulting inhomogeneous tSNR across the brain (blue arrows in Fig. 2(A)). The fact that in 3D-segmented-EPI the entire brain volume has the same effective TI can be advantageous to quantify blood volume in VASO (Cheng et al., 2014a; Hua et al., 2013), to quantify T_1

(Huber et al., 2016b; Marques et al., 2010), or to quantify CBF across slices (Gai et al., 2011; Ivanov et al., 2016b). When the effective inversion time is constant across slices, the functional contrast (e.g. blood nulling) is less biased by incomplete blood nulling, which could hamper CBV quantification in VASO experiments (Glielmi et al., 2009).

The different effective T_1-weighting and the correspondingly different signal across k-space segments in 3D-segmented-EPI, however, can result in inhomogeneous signal distribution across k-space accompanied by image blurring along the second phase encoding direction. To account for this and preserve the available MR signal across k-space segments, a flip angle modulation was used here following previous studies (Gai et al., 2011).

It must be noted, however, that this approach of using variable flip angles can only serve as a first order correction to minimize T_1-related blurring in the second phase-encoding (segment) direction. There are numerous higher-order effects that can not be corrected for with this approach. For instance, the approach of variable flip angles can be optimized for one T_1-compartment, only. Here, the nominal flip angles are adjusted to the T_1 of GM. This means that the blurring effect in WM and CSF are only partly accounted for. Hence the point-spread-function is expected to be different across different tissue types comparable to conventional so-called anatomical sequences like MPRAGE or MP2RAGE. Furthermore, the approach of variable flip angles is limited by the inhomogeneities in RF transmit field at 7T. Hence, in brain regions with particularly high or low B_1^+ field strenghts, the T_1-related blurring effect might be only partially accounted for.

4.3. Benefits of VASO compared to GE-BOLD at lower resolutions

The main benefits of VASO compared to BOLD are its quantifiability (Lu et al., 2003) and local specificity (Jin and Kim, 2006).

The 3 mm protocol used in this study is optimized to obtain fast whole cortex coverage. At these resolutions, it is not expected that CVB-fMRI offers a higher specificity than GE-BOLD (Turner, 2002). However, it might still be beneficial to apply VASO with this protocol, e.g. in studies, when its quantitative nature becomes important (Guidi et al., 2016; Kazan et al., 2015).

The results from the 1.5 mm protocol used in this study show the higher localization specificity to GM of VASO compared to GE-BOLD signal (blue arrows in Fig. 4(I)–(J)). This is consistent with earlier studies (Huber et al., 2016a) and might be advantageous to separate close brain areas (e.g. M1 and S1) in network analysis or to minimize cancellation of positive and negative fMRI responses in neighboring regions (Huber et al., 2016a).

A disadvantage of VASO compared to GE-BOLD is its reduced sensitivity with fewer activated voxels detected (see voxel cluster size in Fig. 4(C)–(D) and (I)–(J)). VASO is furthermore limited by its reduced imaging efficiency, resulting from the acquisition delay that is required for T_1-contrast to develop. Hence, to obtain an artifact-free VASO contrast, TR cannot be reduced to significantly below 3 s. The efficiency of BOLD fMRI, in contrast, is only limited by acquisition speed without comparable dead times as in VASO fMRI.

Considering the different imaging efficiency of the two fMRI methods, senstitivity comparisons between VASO and BOLD contrasts must be interpreted with caution. Here, we can only compare VASO experiments at its optimal TR of 3 s compared to BOLD experiments at the same TR of 3 s. But with the data acquired in this study, we cannot compare optimal VASO experiments with optimal BOLD experiments having shorter TRs of 1 s. For higher temporal resolution in BOLD fMRI, physiological noise can be sampled below the Nyquist rate, which can help to improve the functional sensitivity of BOLD fMRI even further (Stirnberg et al., 2016).

4.4. Effect of head motion

We investigated the effect of head motion during a Valsalva breathholding tasks with 2D-SMS-VASO and 3D-segmented-EPI VASO. We find that having the same effective inversion times across slices in 3D-segmented-EPI-VASO makes it more suitable for restrospective motion correction compared to 2D-SMS-EPI. Results shown in Fig. 5 suggest that even at resolutions of 1.5 mm, where 2D-SMS-VASO provides higher sensitivity than 3D-segmented-EPI-VASO, one might want to refrain from 2D-SMS-VASO applications. It must be noted that the motion artefacts shown in Fig. 5 are most probably referring to head tilting between TRs of the sequence. The artefacts are likely not caused from head tilting during the relatively short acquisition windows. Hence, the apparent motion can be appropriately corrected retrospectively using rigid-body transformations. Motion during the acquisition window itself, however, can result in different artefacts that are harder to correct for (Ladstein et al., 2016). While the 3D-segmented-EPI can better account for contrast inhomogenies across slices compared to 2D-SMS-EPI, this does not mean that it can account better for other shortcomings when head motion is present. For instance, inter-TR and intra-TR head motion will also have a smooting effect in 3D-EPI, while in the 2D EPI there would be fluctuations due to spin history effects.

4.5. Functional specificity

The high-resolution results given in Figs. 3(A), (C), (G), (I) show that VASO fMRI can better delineate individual GM territories compared to GE-BOLD, which shows largest activation between the opposing GM banks of a sulcus. In addition, the specificity within cortical layers and the activity pattern following the cortical ribbon; Fig. 4(G) suggest high localization specificity of CBV-fMRI compared to GE-BOLD signal. This is consistent with previous comparisons of CBV-fMRI and BOLD fMRI (Goense et al., 2007; Huber et al., 2015b; Kim and Ogawa, 2012) and one of the original motivations to do CBV-based fMRI.

4.6. Layer-dependent responses in light of the underlying physiology

For conventional 3 mm voxels, CBF, CBV, and BOLD usually co-vary and are related to oxygen metabolism. With layer-dependent sub-millimeter voxels, however, observed neuro-vascular coupling may be altered (Goense et al., 2012a) and a combined acquisition of BOLD with CBF/CBV-based fMRI methods are required (Huber et al., 2016a) to provide additional information about neurovascular coupling, and to aid modeling and interpretation of high-resolution fMRI (Goense et al., 2016).

As indicated in Fig. 6(E)–(H), at layer-dependent resolutions, vascular and neuronal heterogeneities of the cortex, approach the scale of functional resolutions. Hence, to accurately predict and interpret fMRI responses, some of these features need to be known. This is important in order to model their effect and interpret the results in the light of their respective signal biases (Gagnon et al., 2015; Heinzle et al., 2015; Markuerkiaga et al., 2016).

In BOLD fMRI, variations in the venous baseline blood volume can be problematic. For instance, due to the flow of diluted deoxy-hemoglobin concentrations, large veins that are passing through the upper cortical layers can evoke signal changes distant to the source of the concentration changes. Hence, layer-dependent variations of venous baseline CBV can be considered as a scaling parameter of locally-unspecific functional signal changes (Guidi et al., 2016).

Since VASO is a quantitative contrast that provides local volume results in physical units of ml, it is believed to be less biased towards variations in the vessel structure. Even though there are layer-dependent variations in baseline CBV (see Fig. 6(G)–(H) and (Duvernoy et al., 1981; Weber et al., 2008)), the mere presence of blood vessels does not mean that they introduce a CBV fMRI signal confound during the functional task, like they do in BOLD fMRI. Layer-dependent variations of baseline CBV can be considered as spatially-varying the dynamic range of fMRI responses to the average neural metabolism within each layers.

Aside of potential biases with respect to variations in baseline vasculature, there is a biological limit of mapping neutral activity by means of the hemodynamic response. For microvessels across cortical columns, the spatial limit of neurovascular coupling is in the range of the inter-columnar distance of ≈ 0.5 mm (Blinder et al., 2013). The vascular organization across the cortical depth, however, may be less specific. CBV signal changes in ultra-high resolution animal fMRI is often suggested to be arising from layer-specific micovessels only (Harel et al., 2006; Zhao et al., 2007). Optical studies, however, report of CBV contributions of layer-unspecific diving arterioles (Tian et al., 2010) up to large pial arteries (Kennerley et al., 2012). While their effect on layer-dependent fMRI responses are considered to be much smaller compared to the BOLD signal (Huber et al., 2015b), it has not been conclusively established up to what extent macrovascular CBV contaminations might contribute to layer-dependent CBV fMRI results (Huber et al., 2015a).

4.7. Neuroscientific layer-dependent applications

This study focuses on tackling the technical challenges that need to be met in order to obtain interpretable layer-dependent fMRI responses, and as such, a detailed explanation of the finger-tapping-induced signal in light of neural feed-forward/feedback circuitry (Weiler et al., 2008) is beyond the scope of this paper. Nevertheless, we shall assess the possibility of layer-dependent interpretation with the presented results. There are three major challenges in infering neuroscientific interpretations from high-resolution fMRI data:

4.7.1. Resolution-sensitivity compromise—In animal studies resolutions up to few hundred μm fMRI can be routinely achieved. This can provide layer-specific responses within individual cortical layers. In human layer-dependent fMRI studies, however, currently

achievable resolutions of 0.75 – 0.8 mm are just beginning to unravel groups of cortical layers without considerable partial voluming from CSF of WM. Hence, special care must be taken in order to get even near the resolution of the nominal voxel size. Here, degradation in the effective resolution is sought to be kept as low as possible by minimizing the partial Fourier-factor and T_2^*-related image blurring (Huber et al., 2015c) as well as by avoiding signal interpolation during image registration (Renvall et al., 2016).

The achievable resolution and voxel size of the fMRI acquisition is not only limited by the amount of MRI signal available to detect functional activations in the first place, but mostly by the available gradient power, corresponding acquisition speed and constraints of peripheral nerve stimulations. Hence, even with the high SNR of multi-channel coil arrays and application of advanced acceleration methods, additional challenge remains to acquire the signal in a useful time scale - preferably smaller than the tissue's T_2^*. In the experiments described here, this challenge could be addressed by partly sacrificing the flexibility regarding the FOV dimensions and using slice orientation perpendicular to the cortical surface.

We would also like to stress that the the protocol used here is kept within the parameter space of most 7 T fMRI studies. The total fMRI experiment duration was only 12 min and, therefore, much shorter than most protocols to detect layer-dependent activity. Furthermore, no custom designed scanner hardware was used.

4.7.2. Accuracy of layer-dependent analysis—The interpretation of layer-dependent results averaged over large areas of cortex relies on accurate post-processing including: creation of an accurate surface model, cortical depth estimation, distortion correction etc. For example, the application of so-called 'anatomical sequences', as an anotmical reference with a readouts that are non-distortion matched to the fMRI data, can result in signal smoothing across the cortical depth (Huber et al., 2016b; Renvall et al., 2016). Analogously, imperfections in distortion corrections and signal interpolation during coregistration will result in loss of spatial specificity. Furthermore, inaccurate algorithms used for the estimation the cortical depth can 'introduce' spurious fMRI peaks into cortical profiles that are not really there (Waehnert et al., 2014).

In the study presented here, a strong effort was made to avoid such pitfalls by improving the functional sensitivity to an extent that layer-dependent responses can be seen in single-slice functional maps, without relying on extensive signal averaging over large chunks of cortex. By performing all signal evaluation directly in EPI space, distortion correction and coregistration are rendered unnecessary. Hence, the results shown in Fig. 6. are largely unaffected by inaccurate post-processing.

Based on the considerations above, we conclude that 3D-segmented-EPI VASO provides a promising sequence for neuroscientific studies that use layer-dependent analysis.

4.8. Other fMRI contrast mechanisms

Spin-echo BOLD fMRI has been suggested to have higher specificity to the microvasculature (Bandettini et al., 1994; Uludag et al., 2009) and its utility for laminar

fMRI has been demonstrated in animals (Goense et al., 2012b; Harel et al., 2006; Zhao et al., 2006) and in humans (Yacoub et al., 2005). Until today, SE-BOLD has been the only fMRI method to directly map orientation columns in human visual cortex (Yacoub et al., 2008). However, it suffers from much lower sensitivity, especially at high resolution (Boyacioglu et al., 2014; Budde et al., 2014; Harmer et al., 2012) and practical contraints posed by RF power deposition, which may limit the widespread application of the technique. Future studies with a direct comparison of functional specificity of VASO CBV and SE-BOLD are required to access their applicability to adress neuroscientific layer-dependent questions.

4.9. Other readout strategies

There have been alternative readout strategies proposed to increase the imaging coverage beside 3D-segmented-EPI. For instance, VASO has been combined with imaging readouts including 3D-GRASE, (Lu et al., 2004; Poser and Norris, 2011, 2009), TFL/FFE (Cheng et al., 2014b; Hua et al., 2013), and 3D-HASTE (Poser and Norris, 2007). These 3D-based readout strategies also have the potential of advanced acceleration in both phase-encoding directions with potential CAIPI field-of-view shifting. At high resolutions, however, the readout methods of 3D-GRASE and 3D-HASTE are partly limited by the long readout duration compared to the tissue's T_2, which can result in signal blurring along the second phase-encoding direction (Kemper et al., 2015). Multi-shot, fast GRE readout methods (TFL/FFE), such as used in (Cheng et al., 2014b; Hua et al., 2013), do not have this limitation and could be a promising alternative for 3D-segmented-EPI-VASO at high resolutions. The contrast independent signal acquisition with a fast GRE readout might not only be an suitable approach in combination with VASO imaging (Hua et al., 2013). Encouraging results have also been shown in the elegant combination of a T2-prep module with a fast GRE readout (Hua et al., 2014). Future studies are needed to investigate the functional contrast of this approach compared to VASO at high spatial resolutions.

5. Conclusion

Our results show that for neuroscientific layer-dependent applications, it may be more helpful to refrain from conventional functional contrast (GE-BOLD) and readout strategies (2D-EPI). The challenges of ultra-high resolutions can be optimally addressed with alternative and not yet widespread contrast mechanisms (e.g. CBV) and readout strategies (e.g. 3D-segmented-EPI).

Acknowledgments

We thank Puja Panwar, Benjamin Gutierrez, and Kenny Chung for radiographic assistance. We thank Steve Cauley at MGH for sharing the interface of their image reconstruction for use with the SMS acquisition. The research was supported by the NIMH Intramural Research Program (#ZIA-MH002783). The study was approved under NIH Combined Neuroscience Institutional Review Board protocol #93-M-0170 (ClinicalTrials.gov identifier: NCT00001360). Co-authors contributions were supported by Netherlands Organization for Scientific Research NWO: VIDI 452-11-002 for Kamil Uludağ and Initial Training Network, HiMR, funded by the FP7 Marie Curie Actions of the European Commission (FP7-PEOPLE-2012-ITN-316716) for Maria Guidi. Many thanks to Jozien Goense for continuously consulting us regarding layer-dependent fMRI. We thank Carsten Stueber for providing us the histology slice shown in Fig. 6. We acknowledge Harald Möller for early suggestion to combine VASO with a 3D-EPI readout. The 3D-EPI sequence code used here is based on previously published 3D-EPI sequences (Poser et al., 2010), and we would like to thank Markus Barth for his contributions to earlier versions of this sequence. We

also want to thank Eric Wong for discussions about the mechanisms, where the SNR increase in 3D-acquisitions is coming from. The authors are happy to share the sequence upon request. Preliminary accounts of this work have been presented in the Proceedings of the 24th Annual Meeting of ISMRM, Singapore, 2016 (abstract 944).

Abbreviations

BOLD	blood oxygenation level dependent
CAIPIRINHA (CAIPI)	Controlled Aliasing in Parallel Imaging Results in Higher Acceleration
CBV	cerebral blood volume
CNR	contrast-to-noise ratio
CSF	cerebrospinal fluid
ΔCBV	change in CBV
EPI	echo planar imaging
fMRI	functional magnetic resonance imaging
FOV	field of view
GE	gradient echo
GM	grey matter
ROI	region of interest
SAR	specific absorption rate
SNR	signal-to-noise ratio
SS-SI VASO	slice-selective slab-inversion VASO
TE	echo time
TI	inversion time
TR	repetition time
VASO	vascular space occupancy

References

Bandettini PA, Wong EC, Jesmanowicz A, Hinks RS, Hyde JS. Spin-echo and gradient-echo EPI of human brain activation using BOLD contrast: a comparative study at 1.5 T. NMR Biomed. 1994; 7:12–20. DOI: 10.1002/nbm.1940070104 [PubMed: 8068520]

Blinder P, Tsai PS, Kaufhold JP, Knutsen PM, Suhl H, Kleinfeld D. The cortical angiome: an interconnected vascular network with noncolumnar patterns of blood flow. Nat Neurosci. 2013; 16:889–897. DOI: 10.1038/nn.3426 [PubMed: 23749145]

Boyacioglu R, Schulz J, Müller NCJ, Koopmans PJ, Barth M, Norris DG. Whole brain, high resolution multiband spin-echo EPI fMRI at 7T: A comparison with gradient-echo EPI using a color-word

Stroop task. Neuroimage. 2014; 97:142–150. DOI: 10.1016/j.neuroimage.2014.04.011 [PubMed: 24736172]

Budde J, Shajan G, Zaitsev M, Scheffler K, Pohmann R. Functional MRI in human subjects with gradient-echo and spin-echo EPI at 9.4 T. Magn Reson Med. 2014; 71:209–218. DOI: 10.1002/mrm.24656 [PubMed: 23447097]

Cauley SF, Polimeni JR, Bhat H, Wald LL, Setsompop K. Interslice leakage artifact reduction technique for simultaneous multislice acquisitions. Magn Reson Med. 2014; 72:93–102. DOI: 10.1002/mrm.24898 [PubMed: 23963964]

Cheng Y, van Zijl PCM, Hua J. Measurement of parenchymal extravascular R2* and tissue oxygen extraction fraction using multi-echo vascular space occupancy MRI at 7T. NMR Biomed. 2014a; 28:264–271. DOI: 10.1002/nbm.3250 [PubMed: 25521948]

Cheng Y, van Zijl PCM, Pekar JJ, Hua J. Three-dimensional acquisition of cerebral blood volume and flow responses during functional stimulation in a single scan. Neuroimage. 2014b; 103:533–541. DOI: 10.1016/j.neuroimage.2014.08.025 [PubMed: 25152092]

Cox R. AFNI: Software for analysis and visualization of functional magnetic resonance neuroimages. Comput Biomed Res. 1996; 29:162–173. DOI: 10.1006/cbmr.1996.0014 [PubMed: 8812068]

Donahue MJ, Hoogduin H, van Zijl PCM, Jezzard P, Luijten PR, Hendrikse J. Blood oxygenation level-dependent (BOLD) total and extravascular signal changes and ΔR2* in human visual cortex at 1.5, 3.0 and 7.0 T. NMR Biomed. 2010; 24:25–34. DOI: 10.1002/nbm.1552 [PubMed: 21259367]

Donahue MJ, Stevens RD, de Boorder M, Pekar JJ, Hendrikse J, van Zijl PCM. Hemodynamic changes after visual stimulation and breath holding provide evidence for an uncoupling of cerebral blood flow and volume from oxygen metabolism. J Cereb Blood Flow Metab. 2009; 29:176–185. DOI: 10.1038/jcbfm.2008.109 [PubMed: 18797471]

Duvernoy HM, Delon S, Vannson JL. Cortical blood vessels of the human brain. Brain Res. 1981; 7:519–579. DOI: 10.1016/0361-9230(81)90007-1

Engel SA, Glover GG, Wandell BA. Retintopic organization in human visual cortex and the spatial precision of functional MRI. Cereb Cortex. 1997; 7:181–192. DOI: 10.1093/cercor/7.2.181 [PubMed: 9087826]

Feinberg DA, Beckett A, Chen L. Arterial spin labeling with simultaneous multi-slice echo planar imaging. Magn Reson Med. 2013; 70:1500–1506. DOI: 10.1002/mrm.24994 [PubMed: 24130105]

Feinberg DA, Setsompop K. Ultra-fast MRI of the human brain with simultaneous multi-slice imaging. J Magn Reson. 2013; 229:90–100. DOI: 10.1016/j.jmr.2013.02.002 [PubMed: 23473893]

Feinberg, Da, Moeller, S., Smith, SM., Auerbach, EJ., Ramanna, S., Gunther, M., Glasser, MF., Miller, KL., Uludag, K., Yacoub, E. Multiplexed echo planar imaging for sub-second whole brain FMRI and fast diffusion imaging. PLoS One. 2010; 5:e15710.doi: 10.1371/journal.pone.0015710 [PubMed: 21187930]

Gagnon L, Sakadzic S, Lesage F, Musacchia JJ, Lefebvre J, Fang Q, Yucel Ma, Evans KC, Mandeville ET, Cohen-Adad J, Polimeni JR, Yaseen MA, Lo EH, Greve DN, Buxton RB, Dale aM, Devor A, Boas DA. Quantifying the microvascular origin of BOLD-fMRI from first principles with two-photon microscopy and an oxygen-sensitive nanoprobe. J Neurosci. 2015; 35:3663–3675. DOI: 10.1523/JNEUROSCI.3555-14.2015 [PubMed: 25716864]

Gai ND, Talagala SL, Butman Ja. Whole-brain cerebral blood flow mapping using 3D echo planar imaging and pulsed arterial tagging. J Magn Reson Imaging. 2011; 33:287–295. DOI: 10.1002/jmri.22437 [PubMed: 21274969]

Glielmi CB, Schuchard RA, Hu XP. Estimating cerebral blood volume with expanded vascular space occupancy slice coverage. Magn Reson Med. 2009; 61:1193–1200. DOI: 10.1002/mrm.21979 [PubMed: 19253363]

Glover GH, Lai S. Self-navigated spiral fMRI: Interleaved versus single-shot. Magn Reson Med. 1998; 39:361–368. DOI: 10.1002/mrm.1910390305 [PubMed: 9498591]

Goense JBM, Bohraus Y, Logothetis NK. fMRI at high spatial resolution: Implications for BOLD-models. Front Comput Neurosci. 2016; 10:1–13. DOI: 10.3389/fncom.2016.00066 [PubMed: 26834616]

Goense JBM, Merkle H, Logothetis NK. High-resolution fMRI reveals laminar differences in neurovascular coupling between positive and negative BOLD responses. Neuron. 2012a; 76:629–639. DOI: 10.1016/j.neuron.2012.09.019 [PubMed: 23141073]

Goense JBM, Whittingstall K, Logothetis NK. Neural and BOLD responses across the brain. Wiley Interdiscip Rev Cogn Sci. 2012b; 3:75–86. DOI: 10.1002/wcs.153 [PubMed: 26302473]

Goense JBM, Zappe AC, Logothetis NK. High-resolution fMRI of macaque V1. Magn Reson Imaging. 2007; 25:740–747. DOI: 10.1016/j.mri.2007.02.013 [PubMed: 17499466]

Grgac K, van Zijl PCM, Qin Q. Hematocrit and oxygenation dependence of blood H2O T1 at 7 tesla. Magn Reson Med. 2012; 70:1153–1159. DOI: 10.1002/mrm.24547 [PubMed: 23169066]

Griswold, Ma, Breuer, F., Blamire, AM., Kannengiesser, S., Heidemann, RM., Mueller, M., Nittka, M., Jellus, V., Kiefer, B., Jakob, PM. Autocalibrated coil sensitivity estimation for parallel imaging. NMR Biomed. 2006; 19:316–24. DOI: 10.1002/nbm.1048 [PubMed: 16705632]

Guidi M, Huber L, Lampe L, Gauthier CJ, Möller HE. Lamina-dependent calibrated BOLD response in human primary motor cortex. Neuroimage. 2016; ahead of print. doi: 10.1016/j.neuroimage.2016.06.030

Haacke EM, Lindskogj ED, Lin W. A fast, iterative, partial-fourier technique capable of local phase recovery. J Magn Reson. 1991; 92:126–145. DOI: 10.1016/0022-2364(91)90253-P

Hales PW, Kirkham FJ, Clark CA. A general model to calculate the spin-lattice (T1) relaxation time of blood, accounting for haematocrit, oxygen saturation and magnetic field strength. J Cereb Blood Flow Metab. 2015; 36:370–374. DOI: 10.1177/0271678X15605856 [PubMed: 26661147]

Harel N, Lin J, Moeller S, Ugurbil K, Yacoub E. Combined imaging-histological study of cortical laminar specificity of fMRI signals. Neuroimage. 2006; 29:879–887. DOI: 10.1016/j.neuroimage.2005.08.016 [PubMed: 16194614]

Harmer J, Sanchez-Panchuelo RM, Bowtell RW, Francis ST. Spatial location and strength of BOLD activation in high-spatial-resolution fMRI of the motor cortex: A comparison of spin echo and gradient echo fMRI at 7 T. NMR Biomed. 2012; 25:717–25. DOI: 10.1002/nbm.1783 [PubMed: 21948326]

Heinzle J, Koopmans PJ, den Ouden HE, Ramanna S, Klaas SE. A hemodynamic model for layered BOLD signals. 2015; 125:556–570. DOI: 10.1016/j.neuroimage.2015.10.025

Hua J, Jones CK, Qin Q, van Zijl PCM. Implementation of vascular-space-occupancy MRI at 7T. Magn Reson Med. 2013; 69:1003–1013. DOI: 10.1002/mrm.24334 [PubMed: 22585570]

Hua J, Qin Q, van Zijl PCM, Pekar JJ, Jones CK. Whole-brain three-dimensional T2-weighted BOLD functional magnetic resonance imaging at 7 Tesla. Magn Reson Med. 2014; 72:1530–1540. DOI: 10.1002/mrm.25055 [PubMed: 24338901]

Huber L, Goense JBM, Kennerley AJ, Guidi M, Trampel R, Turner R, Möller HE. Micro- and macrovascular contributions to layer-dependent blood blood volume fMRI: A multi-modal, multi-species comparison. Proceedings of the International Society of Magnetic Resonance in Medicine. 2015a:2114.

Huber L, Goense JBM, Kennerley AJ, Ivanov D, Krieger SN, Lepsien J, Trampel R, Turner R, Möller HE. Investigation of the neurovascular coupling in positive and negative BOLD responses in human brain at 7T. Neuroimage. 2014a; 97:349–362. DOI: 10.1016/j.neuroimage.2014.04.022 [PubMed: 24742920]

Huber L, Goense JBM, Kennerley AJ, Trampel R, Guidi M, Ivanov D, Gauthier CJ, Turner R, Möller HE. Cortical lamina-dependent blood volume changes in human brain at 7 T. Neuroimage. 2015b; 107:23–33. DOI: 10.1016/j.neuroimage.2014.11.046 [PubMed: 25479018]

Huber L, Guidi M, Goense JBM, Mildner T, Trampel R, Schulz J, Eichner C, Turner R, Möller HE. The magnitude point spread function is an inadequate measure of T2*-blurring in EPI. Proceedings of the International Society of Magnetic Resonance in Medicine. 2015c:2056.

Huber L, Ivanov D, Guidi M, Turner R, Uludag K, Möller HE, Poser BA. Functional cerebral blood volumemapping with simultaneous multi-slice acquisition. Neuroimage. 2016a; 125:1159–1168. DOI: 10.1016/j.neuroimage.2015.10.082 [PubMed: 26522423]

Huber L, Ivanov D, Krieger SN, Streicher MN, Mildner T, Poser BA, Möller HE, Turner R. Slab-selective, BOLD-corrected VASO at 7 tesla provides measures of cerebral blood volume reactivity

with high signal-to-noise ratio. Magn Reson Med. 2014b; 72:137–148. DOI: 10.1002/mrm.24916 [PubMed: 23963641]

Huber L, Marrett S, Handwerker DA, Thomas A, Gutierrez B, Ivanov D, Poser BA, Bendettini PA. Fast dynamic measurement of functional T1 and grey matter thickness changes during brain activation at 7T. Proceedings of the Inernational Society of Magnetic Resonance in Medicine. 2016b:633.

Hurley AC, Al-Radaideh A, Bai L, Aickelin U, Coxon R, Glover P, Gowland PA. Tailored RF pulse for magnetization inversion at ultrahigh field. Magn Reson Med. 2010; 63:51–58. DOI: 10.1002/mrm.22167 [PubMed: 19859955]

Ivanov D, Barth M, Uludag K, Poser BA. Robust ACS acquisition for 3D echo planar imaging. Proceedings of the International Society of Magnetic Resonance in Medicine. 2015:2059.

Ivanov D, Poser BA, Huber L, Pfeuffer J, Uludağ K. Optimization of simultaneous multislice EPI for concurrent functional perfusion and BOLD signal measurements at 7T. Magn Reson Med. 2016a; doi: 10.1002/mrm.26351

Ivanov D, Poser BA, Kashyap SS, Gardumi A, Huber L, Uludag K. Sub-millimeter human brain perfusion. Proceedings of the High Field Meeting of the Inernational Society of Magnetic Resonance in Medicine. 2016b:14.

Jesmanowicz A, Bandettini PA, Hyde JS. Single-shot half k-space high-resolution gradient-recalled EPI for fMRI at 3 tesla. Magn Reson Med. 1998; 40:754–762. [PubMed: 9797160]

Jin, T., Kim, S-G. Spatial dependence of CBV-fMRI: a comparison between VASO and contrast agent based methods. Conference Proceedings of the IEEE Engineering in Medicine and Biology Society; 2006. p. 25-28.

Jorge J, Figueiredo P, van der Zwaag W, Marques J. Signal fluctuations in fMRI data acquired with 2D-EPI and 3D-EPI at 7 Tesla. Magn Reson Imaging. 2013; 31:212–220. DOI: 10.1016/j.mri.2012.07.001 [PubMed: 22921734]

Kazan SM, Mohammadi S, Callaghan MF, Flandin G, Huber L, Leech R, Kennerley A, Windischberger C, Weiskopf N. Vascular Autorescaling of fMRI (VasA fMRI) Improves Sensitivity of Population Studies: A Pilot Study. Neuroimage. 2015; doi: 10.1016/j.neuroimage.2015.09.033

Kemper VG, De Martino F, Yacoub E, Goebel R. Variable flip angle 3D-GRASE for high resolution fMRI at 7 tesla. Magn Reson Med. 2015; n/a-n/a. doi: 10.1002/mrm.25979

Kennerley AJ, Harris S, Bruyns-Haylett M, Boorman L, Zheng Y, Jones M, Berwick J. Early and late stimulus-evoked cortical hemodynamic responses provide insight into the neurogenic nature of neurovascular coupling. J Cereb Blood Flow Metab. 2012; 32:468–480. DOI: 10.1038/jcbfm.2011.163 [PubMed: 22126914]

Kim SG, Harel N, Jin T, Kim T, Lee P, Zhao F. Cerebral blood volume MRI with intravascular superparamagnetic iron oxide nanoparticles. NMR Biomed. 2013; 26:949–962. DOI: 10.1002/nbm.2885 [PubMed: 23208650]

Kim SG, Ogawa S. Biophysical and physiological origins of blood oxygenation level-dependent fMRI signals. J Cereb Blood Flow Metab. 2012; 32:1188–1206. DOI: 10.1038/jcbfm.2012.23 [PubMed: 22395207]

Kim T, Shin W, Zhao T, Beall EB, Lowe MJ, Bae KT. Whole brain perfusion measurements using arterial spin labeling with multiband acquisition. Magn Reson Med. 2013; 70:1653–1661. DOI: 10.1002/mrm.24880 [PubMed: 23878098]

Koopmans PJ, Barth M, Norris DG. Layer-specific BOLD activation in human V1. Hum Brain Mapp. 2010; 31:1297–1304. [PubMed: 20082333]

Koopmans PJ, Barth M, Orzada S, Norris DG. Multi-echo fMRI of the cortical laminae in humans at 7 T. Neuroimage. 2011; 56:1276–1285. DOI: 10.1016/j.neuroimage.2011.02.042 [PubMed: 21338697]

Ladstein J, Evensmoen HR, Haberg AK, Kristoffersen A, Goa PE. Effect of Task-Correlated Physiological Fluctuations and Motion in 2D and 3D Echo-Planar Imaging in a Higher Cognitive Level fMRI Paradigm. Front Neurosci. 2016; 10:Article 225.doi: 10.3389/fnins.2016.00225 [PubMed: 27375405]

Langkammer C, Bredies K, Poser Ba, Barth M, Reishofer G, Fan AP, Bilgic B, Fazekas F, Mainero C, Ropele S. Fast quantitative susceptibility mapping using 3D EPI and total generalized variation. Neuroimage. 2015; 111:622–630. DOI: 10.1016/j.neuroimage.2015.02.041 [PubMed: 25731991]

Larkman DJ, Hajnal JV, Herlihy AH, Coutts GA, Young IR, Ehnholm G. Use of multicoil arrays for separation of signal from multiple slices simultaneously excited. J Magn Reson Imaging. 2001; 13:313–317. DOI: 10.1002/1522-2586(200102)13:2<313::AID-JMRI1045>3.0.CO;2-W [PubMed: 11169840]

Lu H, Golay X, Pekar JJ, van Zijl PCM. Functional magnetic resonance imaging based on changes in vascular space occupancy. Magn Reson Med. 2003; 50:263–274. DOI: 10.1002/mrm.10519 [PubMed: 12876702]

Lu H, van Zijl PCM. A review of the development of vascular-space-occupancy (VASO) fMRI. Neuroimage. 2012; 62:736–742. DOI: 10.1016/j.neuroimage.2012.01.013 [PubMed: 22245650]

Lu H, van Zijl PCM. Experimental measurement of extravascular parenchymal BOLD effects and tissue oxygen extraction fractions using multi-echo VASO fMRI at 1.5 and 3.0 T. Magn Reson Med. 2005; 53:808–816. DOI: 10.1002/mrm.20379 [PubMed: 15799063]

Lu H, van Zijl PCM, Hendrikse J, Golay X. Multiple acquisitions with global inversion cycling (MAGIC): a multislice technique for vascular-space-occupancy dependent fMRI. Magn Reson Med. 2004; 51:9–15. DOI: 10.1002/mrm.10659 [PubMed: 14705039]

Lutti A, Thomas DL, Hutton C, Weiskopf N. High-resolution functional MRI at 3 T: 3D/2D echo-planar imaging with optimized physiological noise correction. Magn Reson Med. 2013; 69:1657–1664. DOI: 10.1002/mrm.24398 [PubMed: 22821858]

Mansfield P, Coxon R, Hyklin J. Echo-volumar imaging (EVI) of the brain at 3.0 T: first normal volunteer and functional imaging results. J Comput Assist Tomogr. 1995; 19:847–852. [PubMed: 8537514]

Markuerkiaga I, Barth M, Norris DG. A cortical vascular model for examining the specificity of the laminar BOLD signal. Neuroimage. 2016; 132:491–498. DOI: 10.1016/j.neuroimage.2016.02.073 [PubMed: 26952195]

Marques JP, Kober T, Krueger G, van der Zwaag W, Van de Moortele PF, Gruetter R. MP2RAGE, a self bias-field corrected sequence for improved segmentation and T1-mapping at high field. Neuroimage. 2010; 49:1271–1281. DOI: 10.1016/j.neuroimage.2009.10.002 [PubMed: 19819338]

Menon R, Ogawa S, Strupp J, Anderson P, Ugurbil K. BOLD based functional MRI at 4 tesla includes a capillary bed contribution: echo-planar imaging correlates with previous optical imaging using intrinsic signal. Magn Reson Med. 1995; 33:453–459. DOI: 10.1002/mrm.1910330323 [PubMed: 7760717]

Mildner T, Müller K, Hetzer S, Trampel R, Driesel W, Möller HE. Mapping of arterial transit time by intravascular signal selection. NMR Biomed. 2014; 27:594–609. DOI: 10.1002/nbm.3098 [PubMed: 24610794]

Moeller S, Yacoub E, Olman Ca, Auerbach E, Strupp J, Harel N, Ugurbil K. Multiband multislice GE-EPI at 7 tesla, with 16-fold acceleration using partial parallel imaging with application to high spatial and temporal whole-brain fMRI. Magn Reson Med. 2010; 63:1144–1153. DOI: 10.1002/mrm.22361 [PubMed: 20432285]

Murphy K, Bodurka J, Bandettini PA. How long to scan? The relationship between fMRI temporal signal to noise ratio and necessary scan duration. Neuroimage. 2007; 34:565–574. DOI: 10.1016/j.neuroimage.2006.09.032 [PubMed: 17126038]

Narsude M, Gallichan D, van der Zwaag W, Gruetter R, Marques JP. Three-dimensional echo planar imaging with controlled aliasing: A sequence for high temporal resolution functional MRI. Magn Reson Med. 2016; 75:2350–2361. DOI: 10.1002/mrm.25835 [PubMed: 26173572]

Polimeni JR, Bhat H, Witzel T, Benner T, Feiweier T, Inati SJ, Renvall V, Heberlein K, Wald LL. Reducing sensitivity losses due to respiration and motion in accelerated echo planar imaging by reordering the autocalibration data acquisition. Magn Reson Med. 2016; 75:665–679. DOI: 10.1002/mrm.25628 [PubMed: 25809559]

Poser BA, Ivanov D, Kannengiesser S, Uludag K, Barth M. Accelerated 3D EPI using 2D blipped-CAIPI for high temporal and/or spatial resolution. Proceedings of the International Society of Magnetic Resonance in Medicine. 2014:1506.

Poser BA, Ivanov D, Kemper VG, Kannengiesser SA, Uludag K, Barth M. CAIPIRINHA-accelerated 3D EPI for high temporal and/or spatial resolution EPI acquisitions. Esmrmb. 2013:226.

Poser BA, Koopmans PJ, Witzel T, Wald LL, Barth M. Three dimensional echo-planar imaging at 7 tesla. Neuroimage. 2010; 51:261–266. DOI: 10.1016/j.neuroimage.2010.01.108 [PubMed: 20139009]

Poser BA, Norris DG. Application of whole-brain CBV-weighted fMRI to a cognitiv stimulation paradigm: Robust activation detection in a stroop task experiment using 3D GRASE VASO. Hum Brain Mapp. 2011; 32:974–981. DOI: 10.1002/hbm.21083 [PubMed: 20578174]

Poser BA, Norris DG. 3D single-shot VASO using a Maxwell gradient compensated GRASE sequence. Magn Reson Med. 2009; 62:255–262. DOI: 10.1002/mrm.22000 [PubMed: 19319900]

Poser BA, Norris DG. Measurement of activation-related changes in cerebral blood volume: VASO with single-shot HASTE acquisition. Magn Reson Mater Physics, Biol Med. 2007; 20:63–67. DOI: 10.1007/s10334-007-0068-0

Renvall V, Witzel T, Wald LL, Polimeni JR. Automatic cortical surface reconstruction of high-resolution T1 echo planar imaging data. Neuroimage. 2016; 134:338–354. DOI: 10.1016/j.neuroimage.2016.04.004 [PubMed: 27079529]

Setsompop K, Gagoski Ba, Polimeni JR, Witzel T, Wedeen VJ, Wald LL. Blipped-controlled aliasing in parallel imaging for simultaneous multislice echo planar imaging with reduced g-factor penalty. Magn Reson Med. 2012; 67:1210–1224. DOI: 10.1002/mrm.23097 [PubMed: 21858868]

Smirnakis SM, Schmid MC, Weber B, Tolias AS, Augath M, Logothetis NK. Spatial specificity of BOLD versus cerebral blood volume fMRI for mapping cortical organization. J Cereb Blood Flow Metab. 2007; 27:1248–1261. DOI: 10.1038/sj.jcbfm.9600434 [PubMed: 17213863]

Song AW, Wong EC, Hyde JS. Echo-volume imaging. Magn Reson Med. 1994; 32:668–71. DOI: 10.1002/mrm.1910320518 [PubMed: 7808270]

Stelzer J, Lohmann G, Mueller K, Buschmann T, Turner R. Deficient approaches to human neuroimaging. Front Hum Neurosci. 2014; 8 Article 462. doi: 10.3389/fnhum.2014.00462

Stirnberg R, Huijbers W, Poser BA, Stocker T. Ultra-fast gradient echo EPI with controlled aliasing at 3T: simultaneous multi-slice vs. 3D-EPI. Proceedings of the International Society of Magnetic Resonance in Medicine. 2016:941.

Stüber C, Morawski M, Schäfer A, Labadie C, Wähnert M, Leuze C, Streicher MN, Barapatre N, Reimann K, Geyer S, Spemann D, Turner R. Myelin and iron concentration in the human brain: A quantitative study of MRI contrast. Neuroimage. 2014; 93:95–106. DOI: 10.1016/j.neuroimage.2014.02.026 [PubMed: 24607447]

Tian P, Teng IC, May LD, Kurz R, Lu K, Scadeng M, Hillman EMC, De Crespigny AJ, Arceuil HED, Mandeville JB, Marota JJA, Rosen BR, Liu TT, Boas DA, Buxton RB, Dale AM, Devor A. Cortical depth-specific microvascular dilation underlies laminar differences in blood oxygenation level-dependent functional MRI signal. Proc Natl Acad Sci. 2010; 34:15246–15251. DOI: 10.1073/pnas.1006735107

Triantafyllou C, Polimeni JR, Wald LL. Physiological noise and signal-to-noise ratio in fMRI with multi-channel array coils. Neuroimage. 2011; 55:597–606. DOI: 10.1016/j.neuroimage.2010.11.084 [PubMed: 21167946]

Turner R. How much cortex can a vein drain? Downstream dilution of activation-related cerebral blood oxygenation changes. Neuroimage. 2002; 16:1062–1067. DOI: 10.1006/nimg.2002.1082 [PubMed: 12202093]

Uludag K, Müller-Bierl B, Ugurbil K. An integrative model for neuronal activity-induced signal changes for gradient and spin echo functional imaging. Neuroimage. 2009; 48:150–165. DOI: 10.1016/j.neuroimage.2009.05.051 [PubMed: 19481163]

van der Zwaag W, Buur P, Versluis M, Marques JP. Distortion-matched T1-maps and bias-corrected T1w-images as anatomical reference for submillimeter-resolution fMRI. Proceedings of the International Society of Magnetic Resonance in Medicine. 2016:1233.

Van Der Zwaag W, Marques JP, Kober T, Glover G, Gruetter R, Krueger G. Temporal SNR characteristics in segmented 3D-EPI at 7T. Magn Reson Med. 2012; 67:344–352. DOI: 10.1002/mrm.23007 [PubMed: 21656557]

Waehnert MD, Dinse J, Weiss M, Streicher MN, Waehnert P, Geyer S, Turner R, Bazin PL. Anatomically motivated modeling of cortical laminae. Neuroimage. 2014; 93:210–220. DOI: 10.1016/j.neuroimage.2013.03.078 [PubMed: 23603284]

Weber B, Keller AL, Reichold J, Logothetis NK. The microvascular system of the striate and extrastriate visual cortex of the macaque. Cereb Cortex. 2008; 18:2318–2330. DOI: 10.1093/cercor/bhm259 [PubMed: 18222935]

Weiler N, Wood L, Yu J, Solla SA, Shepherd GMG. Top-down laminar organization of the excitatory network in motor cortex. Nat Neurosci. 2008; 11:360–366. DOI: 10.1038/nn2049 [PubMed: 18246064]

Wong EC. Optimized phase schedules for minimizing peak RF power in simultaneous multi-slice RF excitation pulses. Proceedings of the International Society of Magnetic Resonance in Medicine. 2012:2209.

Worsley, KJ. Statistical analysis of activation images. In: Smith, PJ.PMM, SM, editors. Functional Magnetic Resonance Imaging: An Introduction to Methods. Oxford University Press; 2001.

Wright PJ, Mougin OE, Totman JJ, Peters AM, Brookes MJ, Coxon R, Morris PE, Clemence M, Francis ST, Bowtell RW, Gowland PA. Water proton T1 measurements in brain tissue at 7, 3, and 1.5 T using IR-EPI, IR-TSE, and MPRAGE: Results and optimization. Magn Reson Mater Physics, Biol Med. 2008; 21:121–130. DOI: 10.1007/s10334-008-0104-8

Wu P, Bandettini Pa, Harper RM, Handwerker Da. Effects of thoracic pressure changes on MRI signals in the brain. J Cereb Blood Flow Metab. 2015; 35:1024–1032. DOI: 10.1038/jcbfm.2015.20 [PubMed: 25712496]

Yacoub E, Harel N, Ugurbil K. High-field fMRI unveils orientation columns in humans. Proc Natl Acad Sci. 2008; 105:10607–106012. DOI: 10.1073/pnas.0804110105 [PubMed: 18641121]

Yacoub E, Ugurbil K, Harel N. 2015fMRI at high magnetic field: Spatial resolution limits and applications. Brain Mapping: An Encyclopedic Reference.

Yacoub E, Van de Moortele PF, Shmuel A, Ugurbil K. Signal and noise characteristics of Hahn SE and GE BOLD fMRI at 7 T in humans. Neuroimage. 2005; 24:738–750. DOI: 10.1016/j.neuroimage.2004.09.002 [PubMed: 15652309]

Zahneisen B, Ernst T, Poser Ba. SENSE and simultaneous multislice imaging. Magn Reson Med. 2015; 74:1356–1362. DOI: 10.1002/mrm.25519 [PubMed: 25376715]

Zahneisen B, Poser BA, Ernst T, Stenger VA. Three-dimensional Fourier encoding of simultaneously excited slices: Generalized acquisition and reconstruction framework. Magn Reson Med. 2014; 71:2071–2081. DOI: 10.1002/mrm.24875 [PubMed: 23878075]

Zhao F, Jin T, Wang P, Hu X, Kim SG. Sources of phase changes in BOLD and CBV-weighted fMRI. Magn Reson Med. 2007; 57:520–527. DOI: 10.1002/mrm.21159 [PubMed: 17326174]

Zhao F, Wang P, Hendrich KS, Uludag K, Kim SG. Cortical layer-dependent BOLD and CBV responses measured by spin-echo and gradient-echo fMRI: Insights into hemodynamic regulation. Neuroimage. 2006; 30:1149–1160. DOI: 10.1016/j.neuroimage.2005.11.013 [PubMed: 16414284]

Highlights

- Limitations of sub-millimeter fMRI are discussed
- CBV-sensitive fMRI is combined with 2D and 3D-segmented-EPI imaging
- At ultra-high resolutions, novel contrast and acquisition schemes are needed
- At high-res: 1.) CBV fMRI outperforms GE-BOLD 2.) 3D-segmented-EPI outperforms 2D-EPI
- CBV fMRI based on 3D-segmented-EPI allow layer-dependent fMRI applications

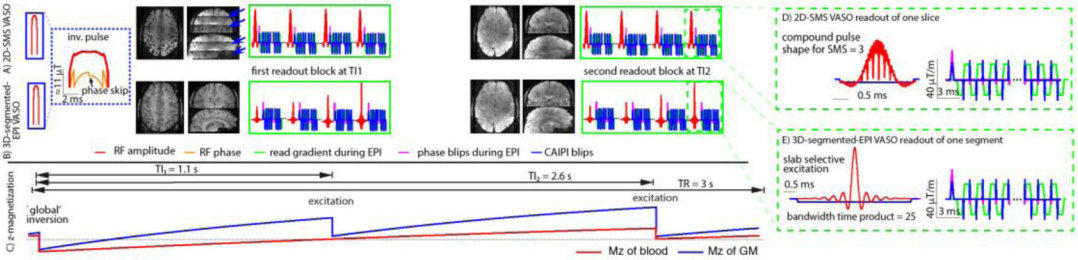

Fig. 1. Magnetization preparation, readout, and sequence timing

Schematic depiction of one TR in the SS-SI-VASO sequence. **(A)** and **(B)** show the timing of the most relevant RF and gradient events for 2D-SMS and 3D-segmented-EPI, respectively. Zoomed views of the corresponding readout modules for individual slices and k-space segments are depicted in **(D)**–**(E)**. Every TR starts with a 'global' adiabatic inversion pulse. A phase skip is used to control the inversion efficiency and the inflow of fast, un-inverted blood. The VASO images are acquired around the blood-nulling time at TI_1 = 1.1 s after successive application of the multi-band/slab-selective RF excitation pulses for 2D-SMS and 3D acquisitions, respectively. The multi-band factor varies between 1 and 3 in this study (SMS-factor = 3 in **(D)**). The phase-encoding and read gradients for the acquisition of the individual slices or k-space segments are accompanied with blipped-CAIPI gradients in slice/segment-direction for controlled aliasing of nearby slices. In this study the corresponding FOV-shift factor varied between 1 and 1/3 (FoV-shift = 1/2 in **(D)**–**(E)**). A second set of images is acquired at TI_2 = 2.6 s containing BOLD-signal-weighting without CBV-weighting. Example brain volumes from every readout are depicted next to their RF and gradient events. Since, the effective TI can vary across slices in the 2D-SMS approach in the range of 200 ms, clear borders of the individual SMS slabs can be seen from the corresponding steps in T_1-weighting (blue arrows in **(A)**).

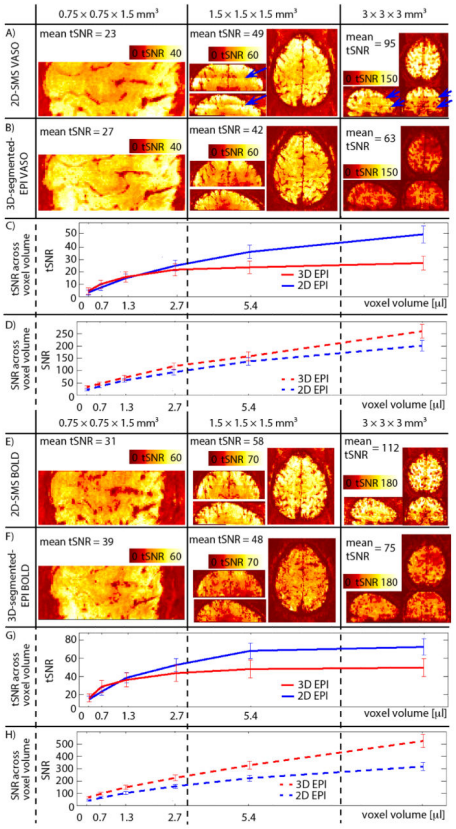

Fig. 2. tSNR across resolutions

Results of VASO tSNR for 0.75 mm, 1.5 mm and 3 mm resolutions are shown for one participant in **(A)**–**(B)**. For the protocols with (low) resolutions of 1.5 mm and 3 mm, 2D-SMS VASO provides higher tSNR values compared to 3D-segmented-EPI. At sub-millimeter resolutions of 0.75 mm, however, the tSNR of 3D-segmented-EPI surpasses that of 2D-SMS EPI. For best visibility, the dynamic range of the color bars is adjusted for each resolution, but it is kept identical for 2D-SMS and 3D-segmented-EPI. tSNR results in **(C)** refer to experiments, where slice-acquisition parameters are kept the same but the slice thickness is varied. Different voxel volumes refer to different slice thicknesses. It can be seen that in the physiological-noise-dominated regime of voxel volumes with few microliters, 2D-SMS-EPI performs better than 3D-segmented-EPI. However, in the thermal-noise-dominated regime at sub-microliters resolutions, 3D-segmented-EPI has higher signal stability. Fig. **(E)**–**(H)** show the same for the BOLD contrast. Similarly to VASO, also the BOLD stability is better for 3D-segmented-EPI at ultra high resolutions, while 2D-SMS is better for conventional resolutions. Note that the ceiling effect is slightly stronger in BOLD compared to VASO. Consequently, the advantage of 3D-segmented-EPI compared to 2D-SMS EPI is visible at smaller voxel sizes only.

All given tSNR/SNR values in **(A)**–**(C)** and **(E)**–**(F)** refer to mean values across participants within ROIs of M1.

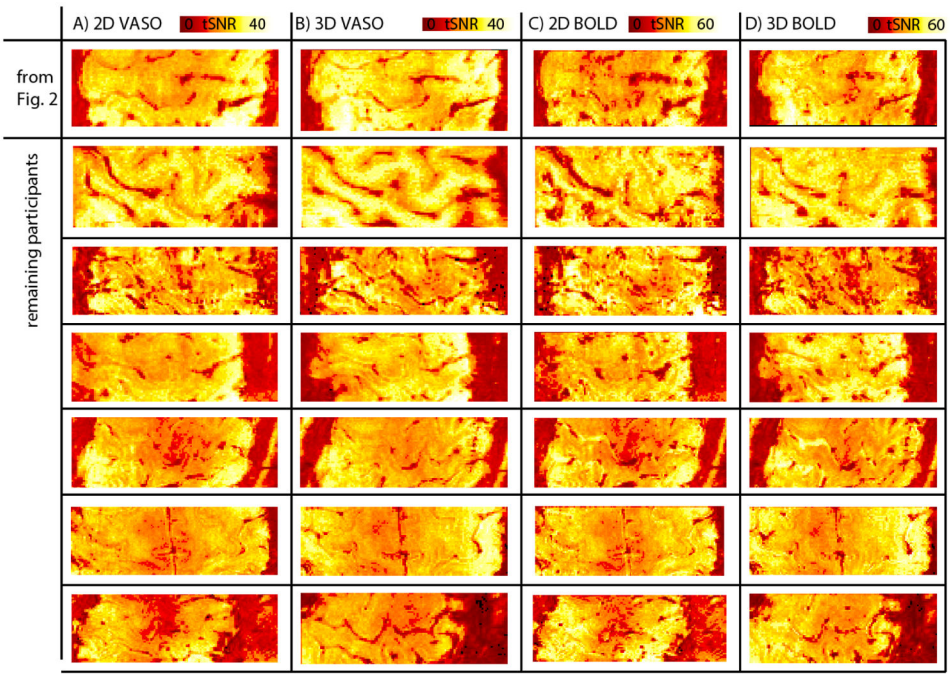

Fig. 3. Stability of tSNR results across participants

The higher temporal stability of sub millimeter voxels shown for one representative subject in Fig. 2 is consistent across participants of the study. For both, BOLD and VASO time series, tSNR values are higher for 3D-segmented-EPI compared to 2D-EPI. Note that BOLD and VASO figures are acquired simultaneously, while 3D-segmented-EPI and 2D-EPI figures are acquired in separate experiments 12 minutes apart. Hence, due to participants head motion between experiment, the slice position can be minimally different. Since the slice positioning and slice tilting was adjusted to be perpendicular to the participants individual M1 cortex, the FOV contains different brain regions for different participants.

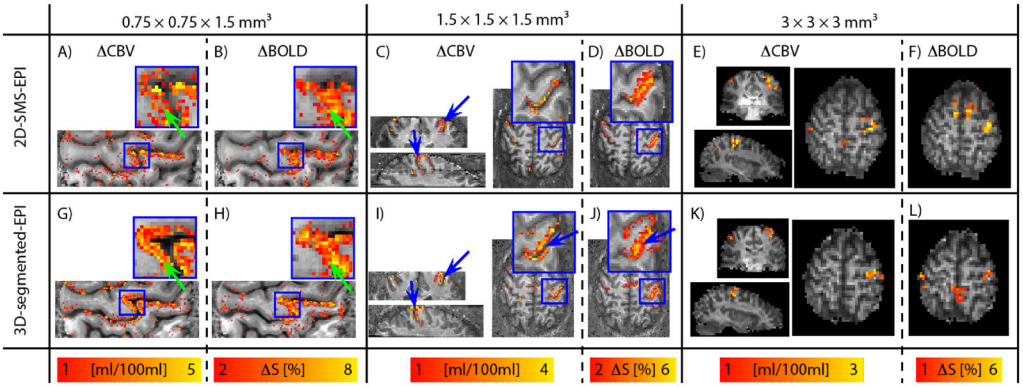

Fig. 4. Functional results across resolutions

Functional activation results for 0.75 mm, 1.5 mm and 3 mm resolutions are shown for one subject in **(A)**–**(F)** for 3D-segmented-EPI and **(G)**–**(L)** for 2D-SMS, respectively. The depicted participant and the depicted slices are the same as shown in Fig. 2 **(A)**–**(B)**. For the sake of comparison, functional maps of BOLD signal changes are shown next to the VASO results. Note that BOLD signal changes are acquired simultaneously with VASO, while 3D-segmented-EPI and 2D-SMS data are acquired in two separate experiments ≈ 14 min apart. Also note that the functional contrasts and the color bars are differently optimized across resolutions, but they are the same for 3D-segmented-EPI and 2D-SMS results. For low resolutions of 3 mm in **(E)**–**(F)** and **(K)**–**(L)**, functional maps don't show strong qualitative differences for contralateral M1. Independent of contrast and readout-strategy, the high tSNR values (Fig. 2) result in sensitivities well above the detection threshold in all cases. At 1.5 mm resolution, the higher specificity of CBV-sensitive fMRI starts to pay off. E.g. two sides of the central sulcus can be better separated with CBV-fMRI compared to BOLD (blue arrows in (**(C)**–**(D)** and **(I)**–**(J)**). At 0.75 mm resolution, layer-dependent activity features become visible in CBV-fMRI results (green arrows in **(A)** and **(G)**), while the BOLD results appear less specific (green arrows in **(B)** and **(H)**).

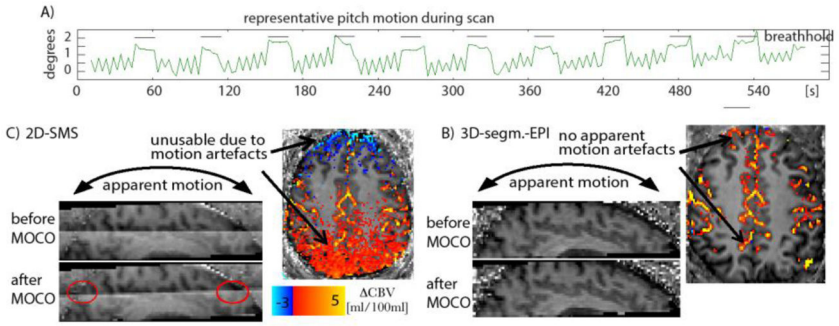

Fig. 5. Susceptibility to task correlated head motion artefacts

Fig. 5 **(A)** depicts the SPM motion parameter of pitch rotation across one representative 10 min Valsalva experiment. The vertical black bars represent the periodes of breathhold. Clear task correlated motion can be seen. The “sawtooth” pattern between breathholding periodes refers to TR locked paced breathing. Fig. **(B)** and **(C)** show the effect of head tilting in 2D-SMS VASO and 3D-segmented-EPI VASO. In 2D-SMS VASO, the different effective inversion time across slices results in different signal intensities. Hence, after retrospective motion correction (MOCO), this signal discontinuity is resampled into agacent slices (red ellypses). This results in task-correlated signal changes visible in the axial plane, rendering any CBV interpretation impossible. In 3D-segmented-EPI VASO on the other hand, the homogenious signal intensity allowes restrospective motion correction without such artefacts.

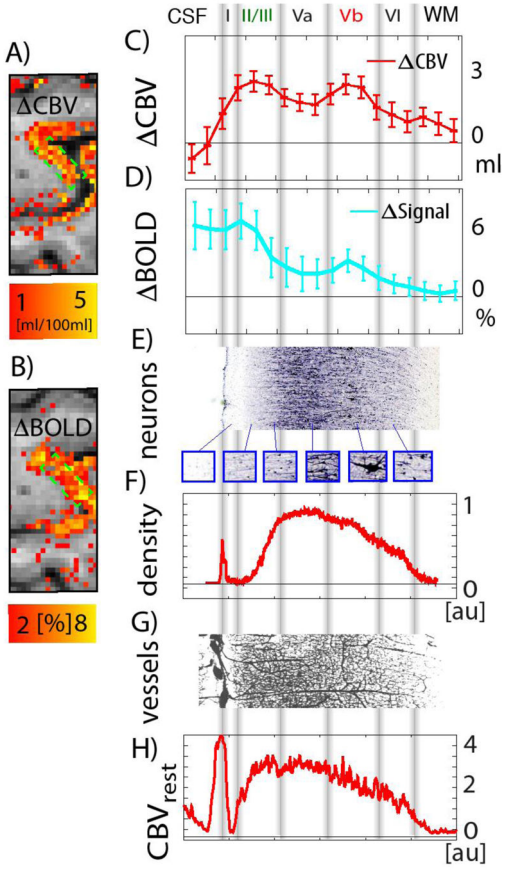

Fig. 6. Usefulness for layer-dependent applications

fMRI responses across cortical depth. **(A)**–**(B)** show the section of the functional activity maps that are used to assess the applicability of VASO and BOLD contrast for layer-dependent fMRI. **(C)**–**(D)** depict the cortical profile of VASO and BOLD signal changes across cortical depth. The VASO signal change appears to be strongest along two cortical depths; upper cortical layers and deeper cortical layers. In BOLD, a similar pattern can be seen, however, it is overlaid on top of a strong gradient of largest BOLD signal change above the cortical surface, decreasing with cortical depth. Data presented in **(A)**–**(D)** refer to the same dataset as schown in Fig. 2 **(B), (F)** and Fig. 4 **(G)**–**(H).** The approximate position of cytoarchitectonically defined cortical layers can be given from stained post-mortem tissue samples (Stüber et al., 2014) (in **(E)** SMI- 311, IHC, cell staining is used). The vertical in this Fig. are manually overlaid based on the different cell types visible in **(E). (F)** portrays the collapsed SMI density plotted as a function of cortical depth, i.e. the y-axis refers to the sum of all gray values within every column of Fig. **(E)**. For most quantitative layer-dependent activity interpretation, the laminar responses must be considered with respect to the baseline vasculature. **(G)** presents the micro vessel distribution of M1 as shown in (Duvernoy et al., 1981). The corresponding baseline CBV is shown in **(H)** as a function of cortical depth. Data shown in **(H)** are derived as the sum of gray values in columns of Fig.

(G). Data shown in **(E)**–**(H)** refer to single-subject post mortem samples and correspond to different individuals as the data acquired in this study **(A)**–**(D)**.